HHS Public Access

Author manuscript

Muscle Nerve. Author manuscript; available in PMC 2017 October 01.

Published in final edited form as:

Muscle Nerve. 2016 October ; 54(4): 763–768. doi:10.1002/mus.25115.

Innervation of dystrophic muscle following muscle stem cell therapy

Matthew Tierney, PhD[3,*], **Christina Garcia, MS**[1,*], **Matthew Bancone, BS**[1], **Alessandra Sacco, PhD**[3], and **Kirkwood E. Personius, PT, PhD**[1,2]

[1]Department of Rehabilitation Science, School of Public Health and Health Professions, University at Buffalo, Buffalo, New York

[2]Program in Neuroscience, School of Medicine and Biomedical Sciences University at Buffalo, Buffalo, New York

[3]Development, Aging and Regeneration Program, Sanford Children's Health Research Center, Sanford Burnham Prebys Medical Discovery Institute, La Jolla, CA

Abstract

Introduction—Duchenne muscular dystrophy (DMD) is caused by the loss of the structural protein, dystrophin, resulting in muscle fragility. Muscle stem cell (MuSC) transplantation is a potential therapy for DMD. Whether donor-derived muscle fibers are structurally innervated is unknown.

Methods—Green Fluorescent Protein (GFP) expressing MuSCs were transplanted into the tibials anterior of adult dystrophic mdx/mTR mice. Three weeks later, the neuromuscular junction was labelled by immunohistochemistry.

Results—The percent overlap between pre- and post-synaptic immunolabeling was greater in donor-derived GFP+ myofibers and fewer GFP+ myofibers were identified as denervated compared to control GFP− fibers ($p = 0.001$ and 0.03, Student's t-test). GFP+ fibers also demonstrated acetylcholine receptor fragmentation and expanded end-plate area, indicators of muscle reinnervation ($P = 0.008$ and 0.033, Student's t-test).

Conclusion—Whether GFP+ fibers are a result of de novo synthesis or fusion with damaged endogenous fibers is unclear. Regardless, donor-derived fibers demonstrate clear histological innervation.

Keywords

Duchenne muscular dystrophy; neuromuscular junction; muscle stem cell

Corresponding author: Kirkwood E Personius, P.T., Ph.D., Dept. of Rehabilitation Science, Kimball Tower Rm. 515, 3435 Main Street, Buffalo, NY 14214-3079, Phone: 716-829-6940; Fax: 716-829-3217; kep7@buffalo.edu.

*These authors contributed equally to the study.

The authors have no financial relationship with the company who manufactures any product or equipment discussed in this manuscript, or any other apparent conflict of interest.

Introduction

Duchenne muscular DMD is an X-linked degenerative disorder which results in progressive muscle wasting beginning in early childhood[1]. DMD is caused by the loss of the cytoskeletal protein dystrophin[2] that serves as a molecular link between cytoplasmic F-actin and β-dystroglycan complex of the sarcolemma[3]. We and others have previously shown that significant structural denervation occurs in the diaphragm of mdx mice[4–7]. These changes include, fragmentation of the acetylcholine endplate into multiple punctate regions, reduced overlap between pre-synaptic nerve terminals and postsynaptic acetylcholine receptors (AChR), and abnormal sprouting of terminal Schwann cell processes (an important component of reinnervation). Interestingly, neurotransmission failure at physiological firing frequencies (35 & 100 Hz) is not increased in these structurally abnormal diaphragmatic neuromuscular junctions (NMJs), but variability of neurotransmission is increased indicating the loss of neuromuscular structure impacts the precision of neurotransmission[5]. Dystrophic muscle is particularly susceptible to eccentric injury[8]. The Lovering lab has shown that following eccentric injury, neurotransmission failure is acutely increased in mdx compared to control mice. The failure in neurotransmission occurs soon after eccentric injury, suggesting a mechanical disruption, rather than newly forming NMJs, as the cause of the transmission failure[9,10]. Thus, the NMJ of dystrophic muscle demonstrate impaired reinnervation and neurotransmission.

MuSC transplantation is a promising therapeutic approach for DMD. Transplantation of stem cell derived myogenic cells in to mdx mice have been shown to increase tissue regeneration and increase muscle force production[11–15]. Since muscle fibers are dependent upon innervation, determining whether dystrophic muscle fibers treated with MuSC are able to maintain their pre-existing innervation or establish new innervation is a critical question. Here, we investigate the structural neuromuscular innervation in the tibialis anterior (TA) muscle of mdx/mTR mice following MuSC transplantation. We report that donor-derived GFP+ muscle fibers demonstrate clear structural innervation.

Methods

Animals

All studies were performed in the TA of 15-week-old mdx/mTR^{G2} mice. Mdx/mTR^{G2} mice have shortened telomeres in addition to a complete lack of dystrophin. These mice demonstrate severe limb muscle degeneration which correlates with the decline in regenerative capacity of the MuSCs[16]. 8-week-old mdx/mTR^{G2} mice demonstrate shorter treadmill run and grid hang times and histological analyses reveals increased heterogeneity of myofiber diameter, mononuclear cellular infiltration, and necrosis[16]. By 24 weeks of age, mdx/mTR^{G2} mice are barely capable of running and start to die at 48 weeks[16]. We chose an age when the TA muscle would be undergoing active bouts of degeneration and regeneration, but would still be functional. All procedures were approved by the Institutional Animal Care and Use Committees of the University at Buffalo and Sanford Burnham Prebys Medical Discovery Institute.

MuSC Isolation and Transplantation

Briefly, MuSCs were isolated by Fluorescent Activated Cell Sorting (FACS) from the TA muscle of green fluorescent protein (GFP) transgenic mice following enzymatic dissociated of nonmuscle tissue as previously described[14,16]. Thus, donor-derived GFP+ have normal dystrophin expression. MuSC were resuspended in PBS and 5,000 or 12,000 GFP+ MuSC were injected intramuscularly into both TA muscles of anesthetized mdx/mTR^{G2} mice. Experimental muscles were harvested 3 weeks after transplantation.

Immunolabeling

Each muscle served as both experimental and control, since GFP+ and GFP− fibers were compared within the same muscle. Hundreds of muscle fibers are visualized in cryosectioned preparations of the TA, thus muscles injected with 5,000 MuSC were used in experiments using cross-sectioned tissue. Muscles were cryosectioned mid-belly (20 μm) and only samples which contained >80% of the muscle were immunolabelled (n = 6 muscles). In order to increase the chance of finding GFP+ fibers, TA muscles which were transplanted with 12,000 GFP+ MuSC were used for muscle whole-mount immunohistochemistry since only superficial muscle fibers can be analyzed in this type of preparation. (n = 6 muscles). For both cryosectioned and whole-mount tissue, the motor nerve axons and terminals were labeled with monoclonal primary antibodies against neurofilaments (2H3) and synaptic vesicles (SV2, Developmental Studies Hybridoma Bank, Iowa City, Iowa). To better visualize GFP+ fibers, GFP was immunolabeled with anti-GFP (Life Technologies). Primary antibodies were visualized with appropriate Alexa Fluor secondary antibodies (Molecular Probes). Postsynaptic AChRs were labeled with rhodamine-alpha-bungarotoxin (Molecular Probes). Cryosectioned muscles were imaged using a Zeiss Axioimager A1 AXiophot microscope at 20× magnification which allows image stitching. Thus, the entire muscle cross-section could be visualized at a relatively high magnification. The NMJ of whole-mount preparations were single plane projections of confocal stacks of images obtained with a Zeiss LSM 510 Meta NLO confocal microscope (63× 1.4 N.A. oil objective).

Quantification of Structural Innervation and muscle cross-sectional area

In cryosectioned muscle preparations, innervation was classified as denervated, weak, or strong (normal). AChR end-plates were classified as denervated when pre-synaptic labeling intensity was no different from background labeling intensity. Innervation was classified as weak when presynaptic labeling was diffuse, but intensity was above background level. Innervation was classified as strong (normal) when pre-synaptic labeling was punctate and intensity was visually clearly above background level. The area of pre-synaptic labeling was determined by identifying the region of overlap between pre-synaptic vesicles and post-synaptic AChR labeling. Muscle whole-mount preparations were used to determine the extent of pre- and post-synaptic overlap (a measurement of structural innervation), the size of the AChR endplate (area), and number of discrete AChR regions per muscle fiber (fragmentation) using previously published methods from our laboratory[4,17]. All measurements were made by a single person blinded to the hypothesized outcomes. To determine the relative size of donor-derived muscle fibers, we measured muscle fiber cross-

sectional area (CSA) and fiber perimeter in GFP+ and nearby GFP− fibers. The same number of GFP+ and GFP− fibers was measured per preparation. Muscle fiber CSA and AChR area were determined using MetaMorph software (Universal Imaging, Downingtown, Pennsylvania).

Statistical Analysis

All values are reported as mean ± SEM unless otherwise noted. A Student t-test was used to compare innervation classification, pre- and post-synaptic overlap, AChR end-plate area, and AChR fragmentation between GFP+ and GFP− muscle fibers. A two-way ANOVA was used to compare differences in muscle fiber CSA and perimeter between GFP+ and GFP− muscle fibers. In the event of a significant ANOVA, a Holm-Sidak post hoc analysis was used for pairwise comparisons. A p-value of ≤ 0.05 was considered significant.

Results

Structural Innervation in muscle cross-sections

TA muscles were cryosectioned and immunolabeled for GFP, AChR, presynaptic vesicles, and neurofilaments (Figure 1). In these mid-belly sections only a small subset of the total number of muscle fibers were sectioned at the level of the NMJ (AChR labeled in red, Figure 1A) and only a small subset of muscle fibers were GFP+ (~10%). Clusters of muscle fibers, most likely in the process of degeneration, demonstrated non-specific Alexa Fluor 647 secondary-labeling (Figure 1A). A total of 507 NMJs from 6 muscles were analyzed (53 from GFP+ fibers and 454 from GFP− fibers). NMJs were classified as structurally denervated (*, no overlap between presynaptic label and AChR receptors above background), weak (<, diffuse overlap between presynaptic label and AChR receptors), or strong (#, bright punctate overlap between presynaptic label and AChR receptors). A limitation of this qualitative analysis is that our results could be affected by location of the muscle section along the endplate band or changes in morphology of the NMJ. Examples of each classification are shown in paired colored and greyscale images in Figure 1 C–H. Denervated muscle fibers were identified in 1.4 ± 0.3% of GFP− fibers, but no denervated fibers were found in GFP+ fibers (Table 1, p = 0.032, one-way t-test). Since denervation is a transient event prior to the fiber disappearing altogether, we are not surprised by this small percentage. 15.5 ± 4.3% of GFP+ fibers showed weak presynaptic labeling compared to 27.8 ± 2.4% of GFP− fibers (Table 1, p = 0.038, one-way t-test). 84.5 ± 4.3% of GFP+ fibers showed strong labeling of nerve terminals compared to 70.8 ± 2.6% of GFP− fibers (Table 1, p = 0.026, one-way t-test). Thus, donor-derived GFP+ myofibers are structurally innervated and the quality of pre-synaptic labeling is similar to GFP− fibers.

NMJ Structure in muscle whole-mounts

To better analyze NMJ histology in donor-derived GFP+ fibers, we used muscle whole-mount preparations to measure the extent of pre- and post-synaptic overlap (structural denervation), endplate AChR area, and counted the number of discrete AChR regions (fragmentation). A total of 106 NMJ from 6 muscle were analyzed (42 GFP+ and 64 GFP− fibers). Figure 2A shows two adjacent GFP− and GFP+ (pseudo-colored blue) fibers. The arrow indicates an area of structural denervation (i.e. post-synaptic region which lacks pre-

synaptic coverage) on the GFP− fiber. GFP+ fibers had greater overlap between pre- and post-synaptic labeling compared to GFP− fibers (Figure 2B Right, 80 ± 2 vs. 62 ± 4%; GFP + vs. GFP−, Student t-test, $p = 0.001$). Since post-synaptic AChR area and muscle fiber CSA are correlated[18], we determined the relative AChR area by normalizing for differences in fiber CSA between GFP+ and GFP− cells. Relative AChR area was significantly greater in GFP+ compared to GFP− muscle fibers (Figure 2B Left, 556 ± 50 vs. 423 ± 23 μm^2; GFP+ vs. GFP−, Student t-test, $p \leq 0.001$). The non-normalized AChR area was 406 ± 37 vs. 423 ± 23 μm^2 for GFP+ vs. GFP−, respectively (Student t-test, $p = 0.674$). Figure 3 shows endplate regions from GFP− and GFP+ fibers. The endplate of GFP− fibers were generally made-up of a few contiguous regions (Figure 3A), but GFP− fibers occasionally show substantial AChR fragmentation (Figure 2A). Since significant degeneration is present in the limb musculature of mdx/mTR^{G2} mice, the presence of some fragmented end-plate regions in control GFP− fibers is not unexpected. The endplates of GFP+ fibers, however, were consistently fragmented (Figure 3B and C) as evidenced by GFP+ endplates averaging 7.2 ± 0.8 discrete regions compared to 5.1 ± 0.6 regions in GFP− endplates (Figure 2B Middle, Student t-test, $p = 0.033$). Expanded post-synaptic AChR area and fragmentation of the AChR end-plate region are both indicators of muscle fiber degeneration and NMJ reinnervation[17,4,19,20]. Thus, donor-derived GFP+ fibers appear to maintain structural innervation during regeneration of endogenous fibers and/or growth of de novo fibers.

Fiber Cross-Sectional Area—Figure 4 A shows example GFP+ and GFP− fibers. GFP+ fibers are visible as the bright fibers within the outlined area. Muscle fiber CSA and perimeter was assessed in 1300 GFP+ and 1300 GFP− fibers from 6 muscles. Muscle fiber CSA was significantly decreased in GFP+ compared to GFP− fibers (889 ± 14 vs. 1107 ± 21 μm^2; GFP+ vs. GFP−, two-way ANOVA, $p \leq 0.001$). Muscle fibers were binned between 0 and 5000 in 200 μm^2 increments. Significant differences were seen between GFP+ and GFP − fibers in 400, 600, 800, and 2400 μm^2 bins (Figure 4B). GFP+ fibers showed a similar decrease in fiber perimeter (106 ± 1 vs. 125 ± 1 μm; GFP+ vs. GFP−, two-way ANOVA, $p \leq 0.001$). Muscle fibers were binned between 0 and 375 in 15 μm increments. Significant differences were seen between GFP+ and GFP− fibers in 60, 75, 90, 195 and 210 μm bins (Figure 4C). Thus, donor-derived GFP+ fibers appear to be growing (de novo myofibers) and/or undergoing regeneration (fusion with endogenous fibers).

Discussion

It has long been known that skeletal muscle is dependent on muscle innervation to maintain contractile function and that denervation results in muscle fiber degeneration[21,22]. Thus, the inability of donor-derived muscle fibers to maintain their innervation or new establish innervation is a potential limitation of stem cell therapy. Our data indicates that donor-derived muscle fibers are structurally innervated and that the extent of pre- and post-synaptic overlap is more extensive when compared to endogenous GFP− fibers, though we acknowledge our analysis of the quality of pre-synaptic labeling in muscle cross-sections preparations may be affected by the altered neuromuscular morphology found in GFP+ fibers. The reduced fiber CSA and perimeter in donor-derived myofibers along with AChR fragmentation and relative expansion of the end-plate are indicators of ongoing muscle fiber

regeneration[23,24]. If GFP+ muscle fibers are undergoing regeneration, then GFP+ fibers would be expected to express embryonic MHC[25]. Since the adult TA predominately contains fast fiber types[26] and endplate area decreases progressively from type IIb, IIx, IIa to I fibers when normalized for fiber diameter, then GFP+ fibers would be expected to have smaller endplate areas compared to GFP− fibers. Our results, however, are the opposite with GFP+ fibers having larger relative areas than GFP− fibers[27]. Thus, the alteration in neuromuscular morphology seen in GFP+ fibers may result from changes in MHC expression during the regeneration process[28]. Taken together, our results suggest that some GFP+ fibers are the result of fusion of MuSC with endogenous fibers during muscle regeneration.

The NMJ appears to be remarkably perdurable in degenerating dystrophic muscles, since neurotransmission failure is not increased in the diaphragm of mdx mice[5]. This functional stability is perhaps due to close interaction between AChRs, rapsyn and utrophin / dystrophin-associated complex at the NMJ[29]. Neuromuscular transmission failure and structural abnormalities, however, can be acutely increased following eccentric injury of limb muscles in mdx mice[9,10]. In sum, severe AChR fragmentation, expanded end-plate area, reduced pre- / post-synaptic overlap, terminal Schwann cell sprouting, and acute neurotransmission failure after muscle injury have been reported in dystrophic muscle[4,5,9,10]. Thus, the NMJ of dystrophic muscle appears to maintain synaptic function despite having significant structural abnormalities. Here, we show that donor-derived muscle fibers, whether via de novo synthesis or fusion with endogenous fibers, also demonstrate clear structural innervation although with structural abnormalities.

Acknowledgments

We are grateful to the National Skeletal Muscle Research Center P30AR061303 and the Engineering for Neurological Rehabilitation Center R24 HD050837-08 (K.E.P & A.S.) for their financial support. We thank Dr. Wade Sigurdson of the Confocal Microscope and Flow Cytometry Facility in the School of Medicine and Biomedical Sciences, University at Buffalo for technical assistance

Abbreviations

DMD	Duchenne muscular dystrophy
MuSC	muscle stem cell
AChR	acetylcholine receptor
NMJ	neuromuscular junction

References

1. Bonilla E, Samitt CE, Miranda AF, Hays AP, Salviati G, DiMauro S, Kunkel LM, Hoffman EP, Rowland LP. Duchenne muscular dystrophy: deficiency of dystrophin at the muscle cell surface. Cell. 1988; 54(4):447–452. [PubMed: 3042151]
2. Hoffman EP, Brown RH Jr, Kunkel LM. Dystrophin: the protein product of the Duchenne muscular dystrophy locus. Cell. 1987; 51(6):919–928. [PubMed: 3319190]
3. Rahimov F, Kunkel LM. The cell biology of disease: cellular and molecular mechanisms underlying muscular dystrophy. J Cell Biol. 2013; 201(4):499–510. [PubMed: 23671309]

4. Personius KE, Sawyer RP. Terminal Schwann cell structure is altered in diaphragm of mdx mice. Muscle Nerve. 2005; 32(5):656–663. [PubMed: 16025531]
5. Personius KE, Sawyer RP. Variability and failure of neurotransmission in the diaphragm of mdx mice. Neuromuscul Disord. 2006; 16(3):168–177. [PubMed: 16483776]
6. Lyons PR, Slater CR. Structure and function of the neuromuscular junction in young adult mdx mice. J Neurocytol. 1991; 20(12):969–981. [PubMed: 1686056]
7. Nagel A, Lehmann-Horn F, Engel AG. Neuromuscular transmission in the mdx mouse. Muscle Nerve. 1990; 13(8):742–749. [PubMed: 2166911]
8. Moens P, Baatsen PH, Marechal G. Increased susceptibility of EDL muscles from mdx mice to damage induced by contractions with stretch. J Muscle Res Cell Motil. 1993; 14(4):446–451. [PubMed: 7693747]
9. Pratt SJ, Shah SB, Ward CW, Inacio MP, Stains JP, Lovering RM. Effects of in vivo injury on the neuromuscular junction in healthy and dystrophic muscles. J Physiol. 2013; 591(Pt 2):559–570. [PubMed: 23109110]
10. Pratt SJ, Shah SB, Ward CW, Kerr JP, Stains JP, Lovering RM. Recovery of altered neuromuscular junction morphology and muscle function in mdx mice after injury. Cell Mol Life Sci. 2015; 72(1):153–164. [PubMed: 24947322]
11. Bareja A, Billin AN. Satellite cell therapy - from mice to men. Skelet Muscle. 2013; 3(1):2. [PubMed: 23369649]
12. Bentzinger CF, von Maltzahn J, Dumont NA, Stark DA, Wang YX, Nhan K, Frenette J, Cornelison DD, Rudnicki MA. Wnt7a stimulates myogenic stem cell motility and engraftment resulting in improved muscle strength. J Cell Biol. 2014; 205(1):97–111. [PubMed: 24711502]
13. Cerletti M, Jurga S, Witczak CA, Hirshman MF, Shadrach JL, Goodyear LJ, Wagers AJ. Highly efficient, functional engraftment of skeletal muscle stem cells in dystrophic muscles. Cell. 2008; 134(1):37–47. [PubMed: 18614009]
14. Collins CA, Olsen I, Zammit PS, Heslop L, Petrie A, Partridge TA, Morgan JE. Stem cell function, self-renewal, and behavioral heterogeneity of cells from the adult muscle satellite cell niche. Cell. 2005; 122(2):289–301. [PubMed: 16051152]
15. Montarras D, Morgan J, Collins C, Relaix F, Zaffran S, Cumano A, Partridge T, Buckingham M. Direct isolation of satellite cells for skeletal muscle regeneration. Science. 2005; 309(5743):2064–2067. [PubMed: 16141372]
16. Sacco A, Mourkioti F, Tran R, Choi J, Llewellyn M, Kraft P, Shkreli M, Delp S, Pomerantz JH, Artandi SE, Blau HM. Short telomeres and stem cell exhaustion model Duchenne muscular dystrophy in mdx/mTR mice. Cell. 2010; 143(7):1059–1071. [PubMed: 21145579]
17. Kulakowski SA, Parker SD, Personius KE. Reduced TrkB expression results in precocious age-like changes in neuromuscular structure, neurotransmission, and muscle function. J Appl Physiol. 2011; 111(3):844–852. [PubMed: 21737823]
18. Balice-Gordon RJ, Breedlove SM, Bernstein S, Lichtman JW. Neuromuscular junctions shrink and expand as muscle fiber size is manipulated: in vivo observations in the androgen-sensitive bulbocavernosus muscle of mice. J Neurosci. 1990; 10(8):2660–2671. [PubMed: 2388082]
19. Balice-Gordon RJ. Age-related changes in neuromuscular innervation. Muscle Nerve Suppl. 1997; 5:S83–S87. [PubMed: 9331392]
20. Fahim MA, Robbins N. Ultrastructural studies of young and old mouse neuromuscular junctions. J Neurocytol. 1982; 11(4):641–656. [PubMed: 7131048]
21. Buller AJ, Eccles JC, Eccles RM. Differentiation of fast and slow muscles in the cat hind limb. J Physiol. 1960; 150:399–416. [PubMed: 13805873]
22. Buller AJ, Pope R. Plasticity in mammalian skeletal muscle. Philos Trans R Soc Lond B Biol Sci. 1977; 278(961):295–305. [PubMed: 19784]
23. Robbins N, Fahim MA. Progression of age changes in mature mouse motor nerve terminals and its relation to locomotor activity. J Neurocytol. 1985; 14(6):1019–1036. [PubMed: 3831242]
24. Robbins N, Nakashiro S. Connections among plasticity, regeneration, and aging at the neuromuscular junction. Adv Neurol. 1993; 59:47–52. [PubMed: 8420122]
25. Charge SB, Rudnicki MA. Cellular and molecular regulation of muscle regeneration. Physiol Rev. 2004; 84(1):209–238. [PubMed: 14715915]

26. Burkholder TJ, Fingado B, Baron S, Lieber RL. Relationship between muscle fiber types and sizes and muscle architectural properties in the mouse hindlimb. J Morphol. 1994; 221(2):177–190. [PubMed: 7932768]

27. Prakash YS, Miller SM, Huang M, Sieck GC. Morphology of diaphragm neuromuscular junctions on different fibre types. J Neurocytol. 1996; 25(2):88–100. [PubMed: 8699198]

28. Stark DA, Coffey NJ, Pancoast HR, Arnold LL, Walker JP, Vallee J, Robitaille R, Garcia ML, Cornelison D. Ephrin-A3 promotes and maintains slow muscle fiber identity during postnatal development and reinnervation. J Cell Biol. 2015; 211(5):1077–1091. [PubMed: 26644518]

29. Shi L, Fu AK, Ip NY. Molecular mechanisms underlying maturation and maintenance of the vertebrate neuromuscular junction. Trends Neurosci. 2012; 35(7):441–453. [PubMed: 22633140]

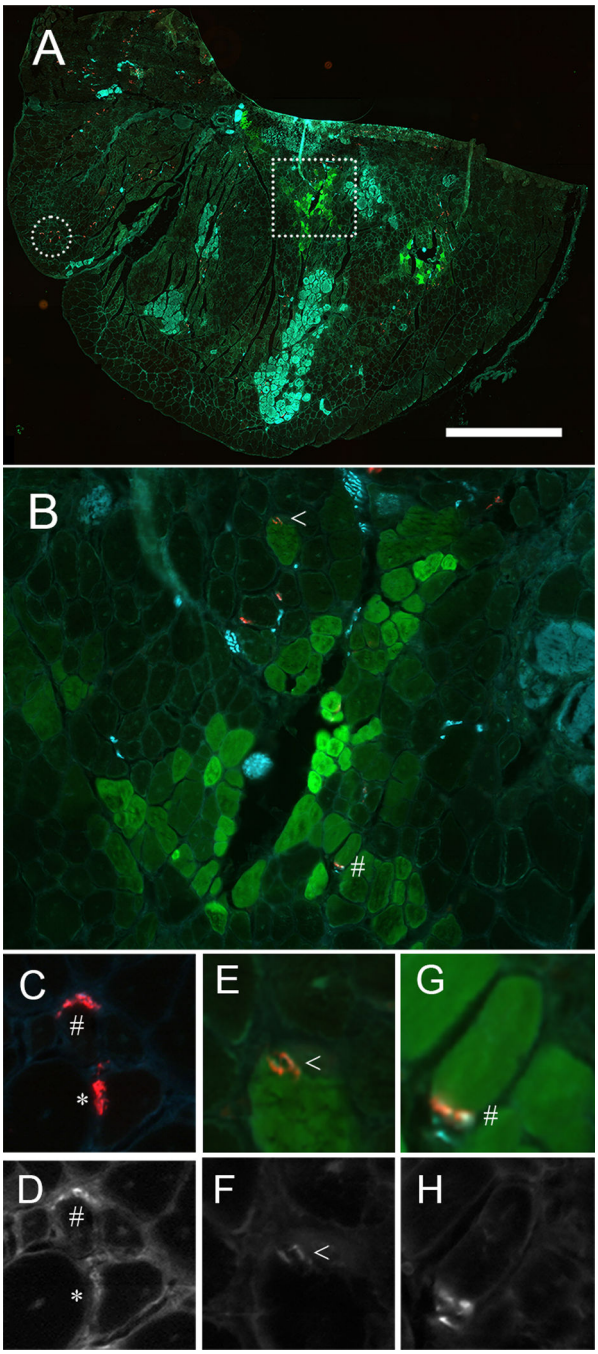

Figure 1.

GFP+ muscle fibers are innervated. **(A)** Cryosection of the tibialis anterior muscle (TA) immunolabeled for GFP (green), postsynaptic acetylcholine receptors (AChR, red) and presynaptic vesicles and neurofilaments (cyan). **(B)** The region marked by the square in A is shown at higher magnification. **(C–H)** Paired color images of pre- and post-synaptic overlap along with greyscale images of presynaptic vesicles and neurofilament label. Neuromuscular junctions were categorized as denervated (*, no overlap between presynaptic label and AChR receptors above background), weak (<, diffuse overlap between presynaptic label and

AChR receptors), or strong (#, bright punctate overlap between presynaptic label and AChR receptors). Fibers shown in C are from the area marked with a circle in A. Fibers shown in E & G are from area marked with a square in A and expanded in B. Scale bar = (A) 1000 μm, (B) 100 μm, and (C) 300 μm.

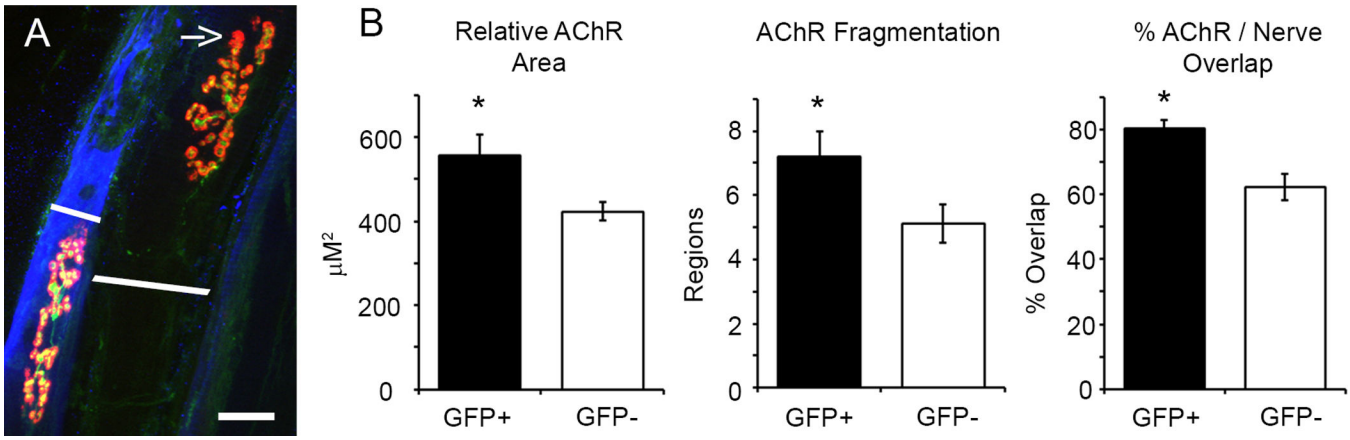

Figure 2.

The NMJ of GFP+ muscle fibers show signs of regeneration but remain innervated. (A) Adjacent GFP− and GFP+ (pseudo-colored blue) muscle fibers. The GFP− fiber shows reduced pre- and post-synaptic overlap (yellow regions) compared to the GFP+ fiber. The arrow indicates a region of structural denervation which lacks pre-synaptic labelling. The white lines show muscle fiber diameter. **(B)** Relative AChR area was increased in GFP+ fibers (556 ± 50 vs. 423 ± 22 μm^2; GFP+ vs. GFP−, Student t-test, p = 0.008).) Some GFP− fibers demonstrated end-plate fragmentation (see example in A), but as a group, GFP+ fibers showed greater AChR fragmentation compared to GFP− fibers (7.2 ± 0.8 vs. 5.1 ± 0.6 regions; GFP+ vs. GFP−, Student t-test, p = 0.033). The extent of pre- and post-synaptic overlap was measured as marker of structural innervation. GFP+ fibers had greater overlap than GFP− fibers (80 ± 2 vs. 62 ± 4%; GFP+ vs. GFP−, Student t-test, p = 0.001). Asterisks indicate significant difference. Scale bar = 20 µm.

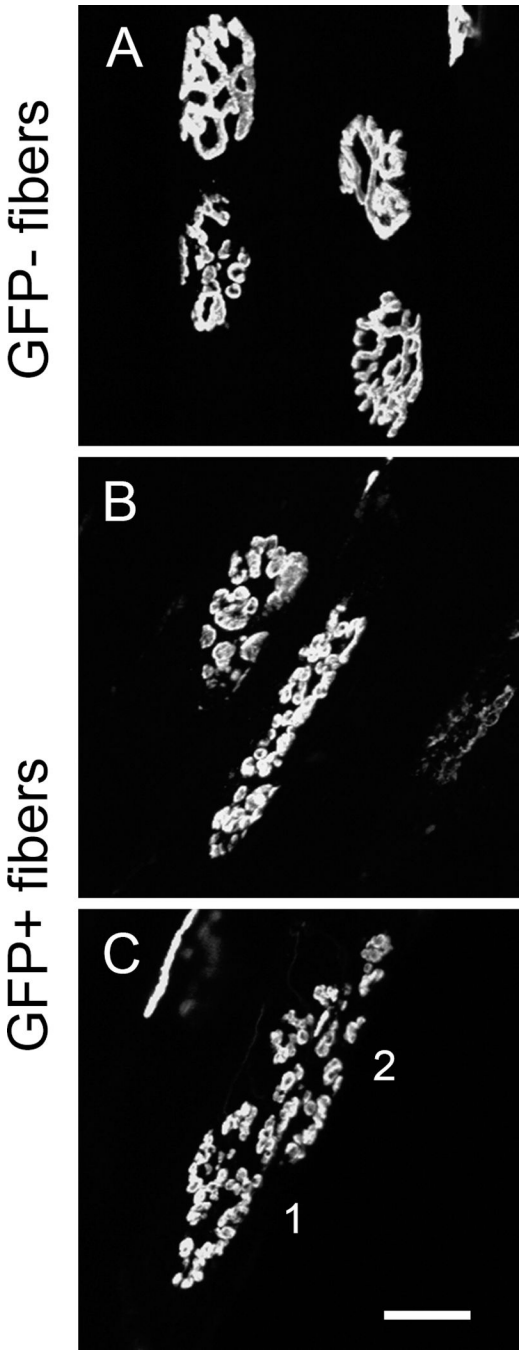

Figure 3.

AChR fragmentation is greater in GFP+ fibers compared to GFP− fibers. (A) Four endplate regions of GFP− fibers showing normal AChR structure. (B &C) GFP+ fibers showed highly fragmented AChR endplate regions. The 1 & 2 in C indicate two distinct muscle fibers. Scale bar = 20 μm.

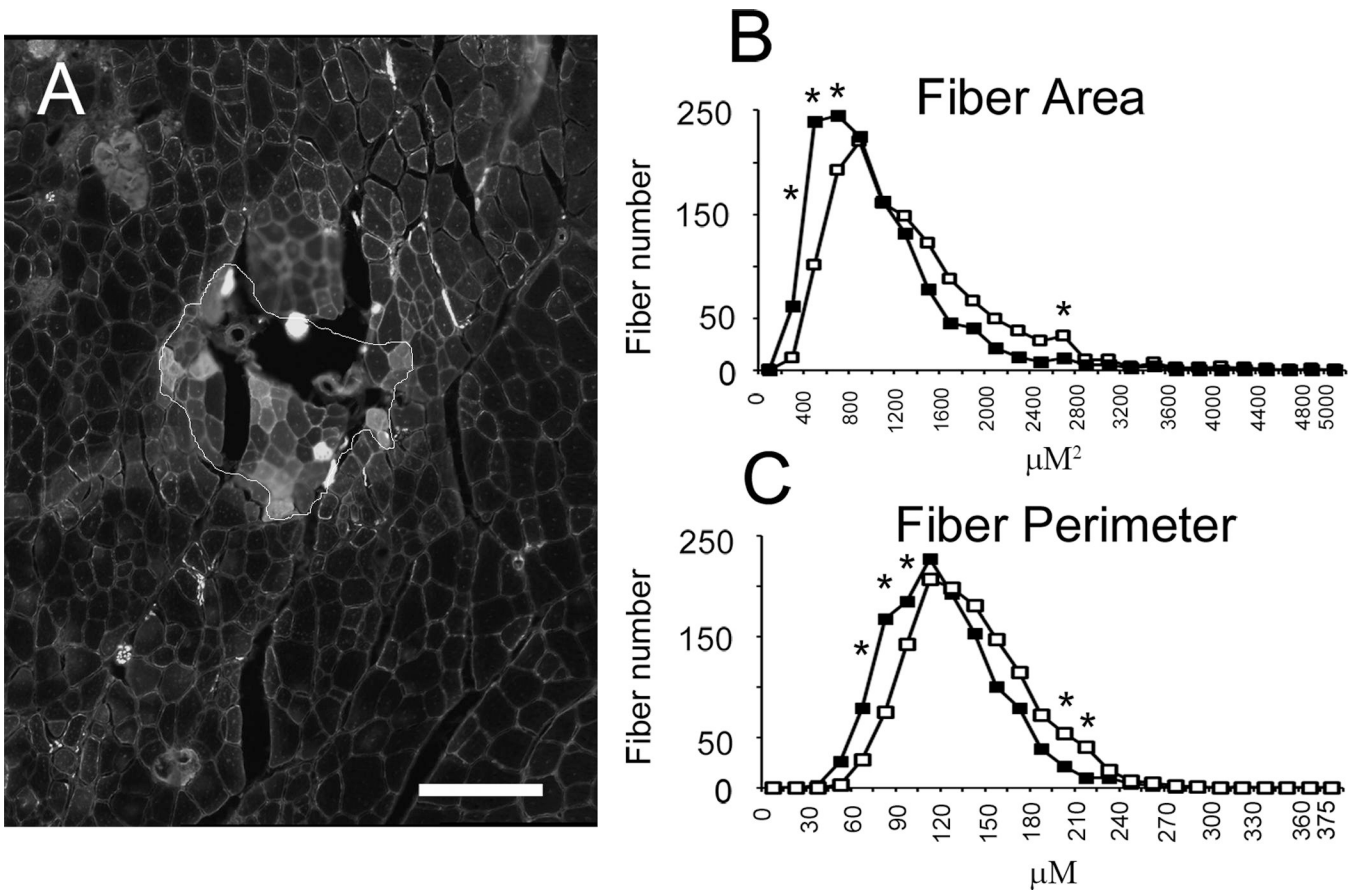

Figure 4.

GFP+ muscle fibers are smaller than GFP− muscle fibers. **(A)** Sample GFP+ and GFP− muscle fibers. GFP+ fibers are visible as the bright fibers within the outlined area. Muscle fiber cross-sectional area (CSA) and fiber perimeter was assessed in 1300 GFP+ and GFP− muscle fibers. Scale bar = 100 μm. **(B)** Frequency histogram of fiber CSA (closed squares are GFP+ fibers, open squares are GFP− fibers). Muscle fiber CSA was reduced in GFP+ fibers (889 ± 14 vs. 1107 ± 21 μm^2; GFP+ vs. GFP−, two-way ANOVA, $p \leq 0.001$). **(C)** Frequency histogram of fiber perimeter. Muscle fiber perimeter was similarly reduced in GFP+ fibers (106 ± 1 vs. 125 ± 1 μm; GFP+ vs. GFP−, two-way ANOVA, $p \leq 0.001$). Asterisks indicate significant difference between GFP+ and GFP− muscle fibers at specific bin sizes.

Table 1

Classification of Pre-synaptic nerve and vesicle labeling

NMJ Classification	GFP+ (%)	GFP− (%)	p-value
Denervated	0 ± 0	1.4 ± 0.3	0.032
Weak labeling	15.5 ± 4.3	27.8 ± 2.4	0.038
Strong labeling	84.5 ± 4.3	70.8 ± 2.6	0.026

mean ± SEM, one-way Student’s t-test